SCIENTIFIC REPORTS

OPEN

SUBJECT AREAS:
CONFOCAL MICROSCOPY
INFRARED SPECTROSCOPY

Received
29 July 2013

Accepted
10 December 2013

Published
10 January 2014

Correspondence and requests for materials should be addressed to C.S. (csoci@ntu.edu.sg)

Mapping polarons in polymer FETs by charge modulation microscopy in the mid-infrared

Xin Yu Chin[1], Jun Yin[1], Zilong Wang[1], Mario Caironi[2] & Cesare Soci[1]

[1]Division of Physics and Applied Physics and Centre for Disruptive Photonic Technologies, Nanyang Technological University, 21 Nanyang Link, Singapore 637371, [2]Center for Nano Science and Technology @PoliMi, Istituto Italiano di Tecnologia, Via Pascoli 70/3, 20133 Milano, Italy.

We implemented spatial mapping of charge carrier density in the channel of a conventional polymer Field-Effect Transistor (FET) by mid-infrared Charge Modulation Spectroscopy (CMS). CMS spectra are recorded with a high sensitivity confocal Fourier Transform Infra-Red (FTIR) microscope by probing electroinduced Infra-Red Active Vibrational (IRAV) modes and low-energy polaron bands in the spectral region 680–4000 cm^{-1}. Thanks to the high specificity and strong oscillator strength of these modes, charge-induced reflectance measurements allow quantitative estimation of charge carrier densities within the FET channel, without the need for amplitude or phase modulation. This is illustrated by identifying the contribution of intrinsic and electrostatically induced polarons to conduction, and by mapping the polaron spatial distribution in a P3HT (Poly(3-hexylthiophene-2,5-diyl)) FET channel under different drain-source bias conditions. This work demonstrates the potential of mid-infrared charge modulation microscopy to characterize carrier injection and transport in semiconducting polymer materials.

Understanding primary charged excitations in conjugated polymers is essential in the optimization of organic semiconductor devices such as light emitting diodes, field-effect transistors (FETs), and photovoltaics, which depend strongly on polaron generation and transport mechanisms. Conventional techniques used for studying polarons in conjugated polymers include photoinduced absorption (PIA)[1–4] and photocurrent (PC)[5–7] spectroscopy. While PIA relies on optical excitation and optical (contactless) probing, PC spectroscopy is based on optical excitation and electrical probing. This allows gathering information on the effects of charge injection and accumulation at the electrodes of working devices. In the last few years, Charge Modulation Spectroscopy (CMS) has emerged as a complementary technique for electrical excitation and optical probing of organic semiconductors. Using this method in a FET device, polaron induced absorption and bleaching features associated to charge carriers are detected upon injection from a metal electrode, without the associated counterions (unlike chemical or photo-doping)[8–15]. Thanks to the highly localized interfacial doping achievable in organic FETs, CMS allows detection of charge carriers in the nanometer-thick accumulation layer, with extremely high sensitivity to polarons[16]. Furthermore, CMS enables discrimination of positive and negative polarons by operating the FET in unipolar mode[17,18], enabling a quantitative estimate of the charge carrier density, that is directly injected into the device, providing two clear advantages compared to the PIA and the PC techniques[15].

Spatially resolving CMS local features along the channel of organic FETs is a unique way to map the injection and distribution of charge carrier density within the thin accumulation region[10,11]. Charge modulation microscopy (CMM) was recently used to probe polaronic features in the n-type FET based on poly{[N,N′-bis (2-octyldodecyl)-naphthalene-1,4,5,8-bis(dicarboximide)-2,6-diyl]-alt-5,5′-(2,2′-bithiophene)} (P(NDI2OD-T2))[19], with confocal monochromatic illumination in the visible and near Infra-Red (IR), revealing local variations on a 0.5 to 1 μm scale that were attributed to different structural conformations of the polymer film[20]. Here, we extend studies of CMM to the mid-IR spectral region to reveal unique vibrational signatures of charge carriers in conjugated polymer FETs[4,8,15].

Electro-induced reflectance is acquired in the mid-IR range by probing electrostatic doping through the appearance of IR Active Vibrational (IRAV) modes and low-energy polaron bands. With an FTIR spectrometer coupled to a confocal microscope, high signal-to-noise ratio CMS spectra are recorded as the difference in the reflectance spectra when the device is in the ON (with charge accumulation) and OFF (without charge

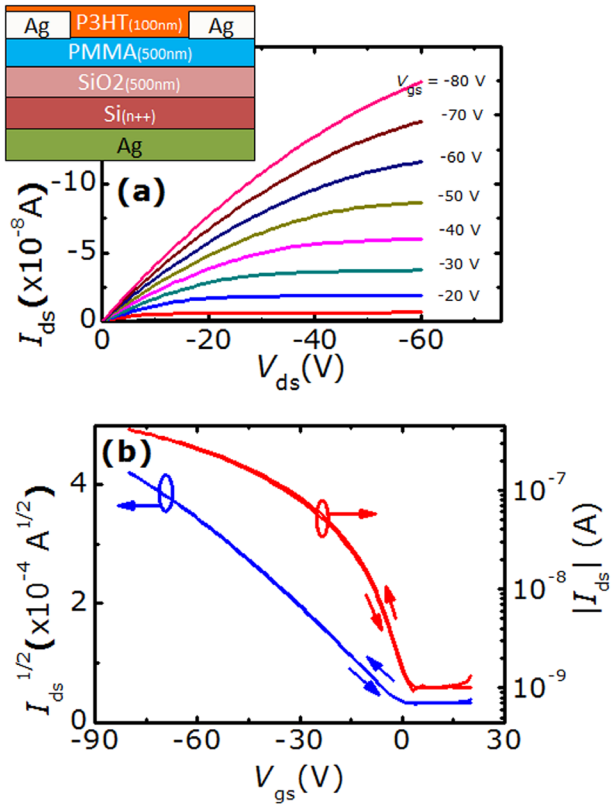

Figure 1 | Typical output (a) and transfer (b) characteristics of P3HT FETs used for CMS studies. Measurements were conducted in inert atmosphere. The device structure is shown in the inset of panel (a), where FET channel length and width are 150 μm and 1 mm, respectively.

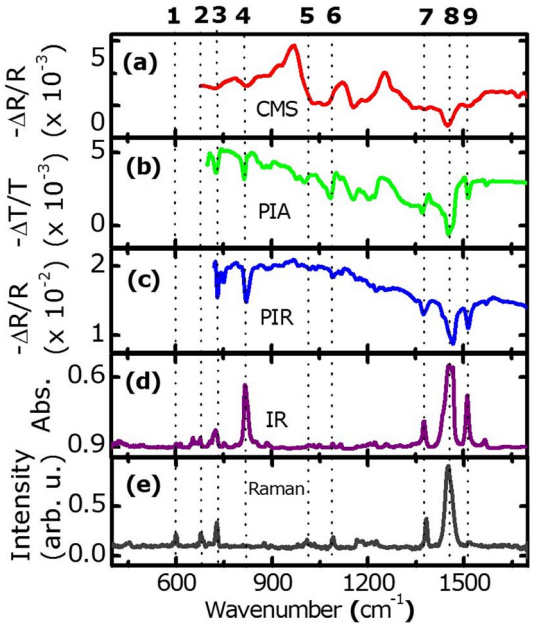

Figure 2 | Comparison of IRAV modes with corresponding IR and Raman vibrational modes of P3HT. (a) Electroinduced reflectance (CMS) spectrum acquired in ambient air condition with $V_{on} = -50$ V, $V_{off} = 25$ V, and $V_{ds} = 0$ V, and averaged 100 times. (b) Photoinduced absorption (PIA) and (c) photoinduced reflectance (PIR) spectra measured at 78 K ($\lambda_{ex} = 532$ nm, $I = 200$ W/cm^2). (d) Room temperature IR absorbance and (e) Raman ($\lambda_{ex} = 532$ nm) spectra. The main vibrational modes are indicated by dashed lines; the numbers on top of panel (a) refer to their labelling in Table 1.

accumulation) state, in an operating FET. Unlike other CMS techniques, where the charge in the channel is modulated around a specific bias point in the ON state and the optical signal is demodulated by lock-in amplifier, our approach allows probing the quasi-static behaviour of the transistor. A similar method was recently adopted to investigate, in the visible and near-IR, water-induced and oxygen induced electron trapping and charge transport instabilities in the n-type polymer semiconductor P(NDI2OD-T2), highlighting the sensitivity of quasi-static acquisition mode to slow and trapped charges[16]. Mid-IR spectromicroscopy has also been previously demonstrated, but with the aid of bright synchrotron radiation and with limited spatial resolution: in this case a V-shape transistor channel had to be employed in order to mimic FETs with different channel lengths and to explore the charge injection length scale[15,21]. By combining the advantages of the diffraction-limited resolution of an FTIR table-top confocal microscope and quasi-static state acquisition of IRAV modes with large oscillator strength (also modelled by Density Functional Theory, DFT), we demonstrate that mid-IR CMS can be used to quantify the electrostatically accumulated charge carrier density and to map the spatial distribution of polarons in the channel of an operating polymer FET device with conventional architecture. As a proof-of-principle, we studied regioregular poly(3-hexylthiophene-2,5-diyl) (P3HT), a polymer largely investigated in optoelectronic and photovoltaic devices[22,23], and its dependence on aging and oxidation in ambient conditions. This shows the potential of IR CMM to address both fundamental and practical issues on charge carrier generation, injection and transport in conjugated polymer materials and devices.

Results

P3HT FETs with the structure shown in inset of Fig. 1 (a) were fabricated to perform CMS studies in back reflection geometry. Typical output and transfer characteristics of these devices (measured in inert atmosphere) are shown in Fig. 1 (a) and (b), from which a saturation mobility (μ_{sat}) of 3.5 × 10^{-3} cm^{2}V^{-1}s^{-1} and a threshold voltage (V_{th}) of 4.1 V can be extracted. The relatively low value of P3HT mobility[4] is due to the presence of PMMA layer at the semiconductor-dielectric interface, which we found necessary to reduce the gate leakage current[24,25] (see Methods and Supplementary Information sections). Overall the devices show suitable characteristics for CMS measurements and low hysteresis, indicative of slow trapping relaxation of induced charges and limited migration of low-mobility dopant ions towards the accumulation layer[26].

The metal-insulator-semiconductor structure of FET devices allows inducing an electrostatic doping at the semiconductor-dielectric interface by applying a suitable voltage to the gate, similarly to photo-induced doping by optical excitation used in PIA studies. CMS spectra are obtained from the change in reflectivity induced by carrier accumulation in the device channel.

Figure 2 shows the comparison between mid-IR PIA spectra measured in conventional transmission geometry (b), somehow unconventional back reflection geometry (c), and CMS spectra in back reflection geometry (a) (see details in the methods section). Absorption and Raman vibrational spectra are also shown in (d) and (e) for reference, and the principal modes are marked by dashed lines and numbered on top of panel (a) according to the labelling in Table 1.

Although an analytical theory of IRAV modes in conjugated polymers has been previously developed, enabling the prediction of the main spectral features of Fano antiresonances, including frequencies, oscillator strengths and relative intensities[27,28], here we employ an *ab-initio* numerical approach, based on DFT, to model their key features. Table 1 summarises experimental and calculated IR, photo-induced (PIA) and charge-induced (CMS) IRAV, and Raman mode frequencies of the main transitions, together with the corresponding

Table 1 | Summary of the experimental and calculated (in bracket) IR, photoinduced (PIA) and electroinduced (CMS) IRAV and Raman mode frequencies for the main transitions of P3HT, along with their vibrational modes assignment

Modes No	IR (cm^{-1})	Assignments	PIA-IRAV (cm^{-1})	CMS-IRAV (cm^{-1})	Raman (cm^{-1})	Assignments
1					599 (595)	C_α-S-C_α ring deformation
2			678		678 (661)	C_α-S-C_α symmetric deformation
3	726 (720)	Hexyl rocking vibration	725	726	727	C_α-S-C_α asymmetric deformation
4	817 (815)	C_β–H out-of plane vibration	817	821		
5			1002		1005	C_β–C_{alkyl} stretching
6			1084	1033,1066	1090	C_α–H and C_β–H bending
7	1378 (1386)	Terminal CH_3	1375	1379	1383 (1358)	C_β-C_β symmetric stretching
8	1456 (1451)	C_α=C_β symmetric stretching	1450	1450	1450 (1430)	C_α=C_β symmetric stretching
9	1512 (1500)	C_α=C_β asymmetric stretching	1512	1514	1512 (1512)	C_α=C_β asymmetric stretching

vibrational modes seen in Fig. 2. Details on the calculations will be published elsewhere.

Figure 3 shows sequential FET transfer curves (a) and corresponding CMS spectra (b) obtained in ambient condition. The time between consecutive runs is approximately 30 minutes. Oxidation of P3HT upon exposure to oxygen and moisture and bias stress in ambient condition is known to increase FET current over time and to cause hysteresis, due to the creation of trap states[29–31], while oxidation-induced doping turns the transistor from normally OFF (i.e. the transistor is OFF at 0 V between gate and source) to normally ON[24,29,32]. This causes a notable shift in threshold voltage ΔV_{th}, compared to pristine devices, that tends to saturate over time (Fig. 3 (c)). Similarly, the IRAV features in CMS spectra, recorded with constant gate voltages $V_{on} = -60$ V and $V_{off} = 100$ V and grounded drain and source electrodes ($V_{ds} = 0$ V), increase in intensity over time and eventually saturate (Fig. 3 (b)), with similar behaviour shown by the antiresonance peak around 1730 cm^{-1} due to the C=O double bond[33] in Fig. 3 (b). This indicates that CMS measurements are indeed sensitive to the increase of charge carriers in the channel and chemical changes induced by electrostatic doping. To quantify these effects, we calculate the effective spectral density of IRAV modes $N_{eff} = \int |-\Delta R/R| d\omega$[14,15], where the integral of the absolute value of CMS spectra is computed between 680 and 1700 cm^{-1} wavenumbers, i.e. in the region containing all IRAV modes according to Raman experiment and DFT calculations. This is plotted in Fig. 3 (c) as doping-induced effective spectral density, $N_{eff,doping} = N_{eff} - N_{pristine}$, after subtraction of the effective spectral density contributed by the device in pristine condition (run #1). As shown in Fig. 3 (c), $N_{eff,doping}$ and ΔV_{th} behave very similarly, suggesting their common origin related to the increase of polarons upon chemical-induced doping of the device.

The doping-induced carrier density can be independently estimated by a simple capacitive model of the FET:

$$\rho_{2D} = \frac{\kappa \varepsilon_0}{eL} \Delta V_{th} \quad (1)$$

The capacitance per unit area of the dielectric composed of 500 nm PMMA (polymethyl methacrylate) on top of 500 nm SiO_2 is estimated to be ~2.8 nF cm^{-2}. Carrier density can therefore be calculated as a function of the measured threshold voltage shifts at each run. To retrieve the correlation between the accumulated carrier

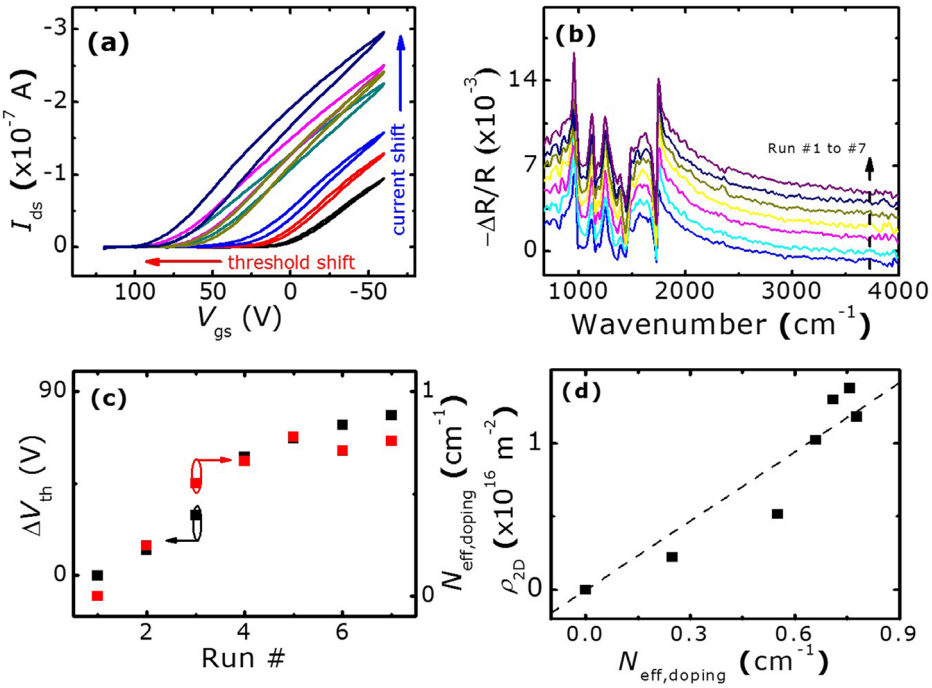

Figure 3 | Aging of P3HT FET under continuous operation in ambient conditions and its signatures in CMS spectra: (a) consecutive transfer characteristics recorded at $V_{ds} = -60$ V. (b) consecutive CMS spectra in ambient air condition with $V_{on} = -60$ V, and $V_{ds} = 0$ V, $V_{off} = 100$ V (spectra are offset by 10^{-3} for clarity). (c) Increase and saturation of doping-induced effective carrier density ($N_{eff} = \int |-\Delta R/R| d\omega$, integrated from 680 to 1700 cm^{-1}) and ΔV_{th} as a function of run number. (d) Linear dependence of ρ_{2D} on $N_{eff,doping}$, which is used to quantify polaron density from CMS measurements.

density and the effective spectral density of IRAV modes, ρ_{2D} can be plotted as a function of the corresponding $N_{eff,doping}$ obtained from CMS measurement, as done in the Fig. 3 (d). A linear fit to the data (dotted line) yields a proportionality constant of 1.57×10^{16} carriers/m^2 per wavenumber (cm^{-1}), which directly relates integrated signal of CMS spectra to polaron density in the device.

Besides estimating the accumulated charge density, one can also retrieve the spatial distribution of charge carriers across the channel of the FET device by hyperspectral mapping. While this was already accomplished in the visible and near-IR spectral range[11,20], previous work on mid-IR polaron mapping had to rely on large-area devices and V-shaped electrodes to determine the charge injection landscape[15]. Here we implement CMS using a high-sensitivity FTIR confocal microscope, which allows "true" hyperspectral mapping by scanning the IR beam across the active channel of a conventional FET device with parallel source-drain electrodes. For these measurements, the gate bias modulation was fixed at $V_{on} = -60$ V and $V_{off} = 80$ V, while the drain-source bias was varied between 0 and -120 V ($V_{ds} = 0, -30, -60, -90, -120$ V). With these measuring conditions, i.e. making sure that the gate bias in OFF is always kept above threshold voltage of the device ($V_{off} < V_{th} \sim 100$ V for this particular device), even if the sample is slightly oxidized throughout the mapping in ambient conditions, CMS spectra remain unaffected over time and depend solely on carriers induced in the channel within each modulation cycle. Evidence for this behaviour is given in Supplementary Information, Fig. S 2 and Table S 1, where CMS spectra and transistor saturation mobility are shown to be constant over time despite the notable shift in threshold voltage.

The profile of charge carrier density (ρ_{2D}) as a function of distance from the drain electrode (x_d) is shown in the three-dimensional plot in Fig. 4 for different values of the source-drain bias (V_{ds}). Carrier density values are deduced from the linear correlation (Fig. 3 (d)) of FET capacitive model and effective spectral density of IRAV modes (corresponding CMS spectra are available as Supplementary Information, Fig. S 3). In these measurements the beam spot size was ~40 μm and the beam was scanned in steps of 20 μm across the contact electrodes. From Fig. 4, notable decrease in carrier density when x_d is lower than 40 μm and higher than 100 μm is due to partial reflection of the IR beam by the metallic electrodes convoluted with the actual differential reflectance from the P3HT active region. Improvement in spatial resolution is possible by decreasing the beam spot size down to the diffraction limit, but at the expense of signal to noise ratio or of an increased overall acquisition time (currently 3 hours for the entire mapping). The graph shows that, when V_{ds} is lower than -90 V, a fairly constant polaron density of $\sim 3 \times 10^{16}$ carriers/m^2 is observed throughout the FET channel. However, for $V_{ds} \geq -90$ V the spatial distribution of the charges varies across the channel, and their density reduces significantly at the drain side. This can be attributed to the decrease in local potential near to the drain electrode, which lowers the density of accumulated charges, similar to previous observations reported in the literature[10,20].

Discussion

Consistent with the previous reports on mid-IR CMS[8], the CMS spectrum in Fig. 2 (a) contains all the IRAV modes typical of PIA spectra of P3HT, which are also shown in Fig. 2 (b) and (c). This confirms the equivalence of interfacial doping by polaron accumulation and photo-doping by optical excitation, and validates our approach of using back reflectance geometry for CMS and PIA measurements on opaque substrates in mid-IR. The IRAV modes observed in CMS and PIA spectra have one-to-one correspondence with vibrational IR and Raman modes in Fig. 2 (d) and (e). IRAV modes stem from symmetry breaking due to the strong coupling between self-localized polarons on the polymer backbone and the local chain distortion, which transforms even parity Raman-active vibrational modes into odd-parity IRAV modes[2,34]. In regioregular

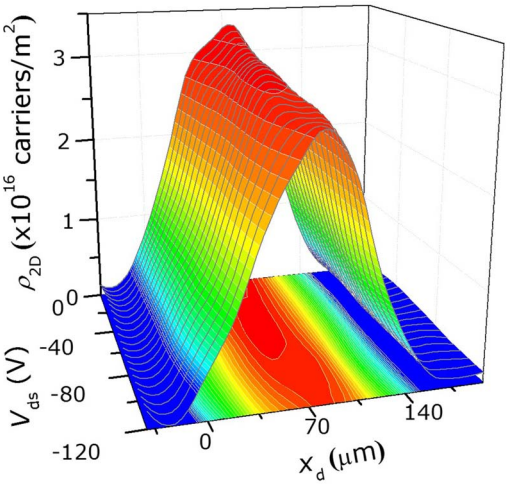

Figure 4 | Three dimensional plot of the charge carrier density distribution across the channel of the polymer FET as a function of different applied source-drain voltage V_{ds} (y-axis). The charge carrier density ρ_{2D} (z-axis) is obtained from analysis of the IR-CMS spectra. x_d (x-axis) is the distance from the drain electrode. Measurements were obtained with gate modulation voltages of $V_{on} = -60$ V and $V_{off} = 80$ V. Note the logarithmic color scale.

P3HT with relatively high charge-carrier mobility, this change manifests itself in the appearance of sharp Fano antiresonances in PIA and CMS differential spectra (indicated by the dashed lines in Fig. 2) in the region of overlap with the broad polaron induced DP1 absorption, typically found around 1100 ± 500 cm^{-1} [4,8,28,35]. IRAV modes describe charge oscillations along the polymer chain and show unusually large oscillator strength[2,36,37], thus providing a very selective and sensitive probe for polaron density and distribution in CMM experiments.

Previous observations of the saturation of effective IR-CMS spectral density as shown in Fig. 3 (c) were discussed in terms of leakage current through the gate (whereby additional leakage current does not increase the CMS signal proportionally) or through possible metal-insulator transition induced in polymer FETs at high carrier densities[15]. Care was taken in our case to reduce significantly the leakage current by means of the additional dielectric PMMA interfacial layer ($I_g \sim -1$ nA at $V_g = -80$ V, see supplementary Fig. S 1). Moreover, metal-insulator transition is expected to result in monotonic Drude-like far-IR absorption typical of delocalized polaron states[14], which was not present in our spectra. The observed signal saturation in Fig. 3 (c) is simply linked to the saturation in the threshold voltage shift with time. This indicates that metal-insulator transition in polythiophene does not occur at carrier densities lower than 10^{16} holes/cm^2, the highest that could be achieved in this work.

In conclusion, mid-IR CMS in reflectance mode was implemented to study the active channel of a working P3HT FET. Polaronic features and IRAV modes with large oscillator strength are observed in mid-IR CMS spectra (680–4000 cm^{-1}) and their assignment is analysed by comparison with vibrational and Raman signatures and DFT calculations. A simple capacitive model allows correlating IRAV CMS spectra to charge carrier density quantitatively, and different gate bias modulation schemes enable identification of signals contributed by oxidation-induced or electrostatically-induced charge carriers. No evidence of a metal-insulator transition is observed at the maximum carrier densities of $\sim 3 \times 10^{16}$ holes/cm^2 achieved here. Lastly, thanks to its high sensitivity and selectivity, CMS reflectance mapping proved valuable to study the spatial distribution of carrier density within the polymer FET device and provided evidence for charge accumulation in the corresponding operating regime of the transistor.

Methods

FET fabrication: A heavily n-doped Silicon wafer (denoted as n^{++}-Si) with 500 nm thermally grown Silicon Dioxide (SiO_2) is treated in ultrasonic bath with acetone and isopropanol for 10 minutes each. 500 nm of PMMA (MW=950,000, 4% in anisole, Microchem) is spincoated on the SiO_2 surface and hardbaked at 180°C for 30 minutes[24]. Control experiments were conducted to make sure that the organic PMMA layer does not contribute to the measured CMS signals (supplementary Fig. S 4). After the spin-coating and hardbaking of PMMA dielectric layer, silver electrodes are deposited by using a metal shadow mask. In this work, silver is adopted as electrodes deposited on the n^{++}-Si side for improving the contact of the gate. Highly regioregular Poly (3-hexylthiophene-2,5-diyl) (Rieke Metals, Inc. BASF's Sepiolid P200, molecular weight ~20–40 K) is used as purchased, without any further purification. 8 mg/ml P3HT solution is prepared using 1,2-Dichlorobenzene (DCB) (Sigma Aldrich) as solvent and is spin-coated at 800 rpm for 120 s. After that, the sample is thermally annealed at 150°C for 10 minutes[38]. The thickness of P3HT is estimated to be around 100 nm by tapping mode AFM. A schematic of the cross-section of the fabricated FET devices is shown in the inset of Fig. 1 (a).

Infra-Red Absorption: Absorption spectra are obtained using a Fourier Transform Infra-red (FTIR) spectrometer (Bruker Vertex 80 v) equipped with RT-DTGS detector. Spectral and phase resolution used during Fourier transformation are 4 and 32 cm^{-1}, respectively.

Photo-Induced Absorption (PIA) and Reflection (PIR): PIA and PIR spectra are obtained at low temperature (T = 78 K) by photoexciting the samples with at continuous wave green laser (λ_{ex} = 532 nm) and probing the induced change in transmission ($-\Delta T/T$) or reflection ($-\Delta R/R$) by an FTIR spectrometer (Bruker Vertex 80 v) equipped with an MCT detector. Thick (~3 μm) P3HT films were drop-cast on KBr substrates for both IR-PIA measurements in transmission mode and PIR measurements in near-normal back scattering geometry. Spectral and phase resolution used during Fourier transformation are 4 and 32 cm^{-1}, respectively. The differential signal of over 5000 consecutive scans with pump light on and off was averaged to increase the signal to noise ratio.

Raman Spectroscopy: Raman spectra were obtained in a Renishaw Raman microscope configured with a charge coupled device array detector. A green (λ_{ex} = 532 nm) laser line was used for excitation with power below 1 μW. Raman signals were collected by a Leica 100× objective lens (NA = 0.85) and dispersed by 2400 line/mm gratings with frequency resolution of ~0.8 cm^{-1}. Integration time was 20 s.

Charge Modulation Spectroscopy: Electrical characterization is carried out by using two Keithley 6487 voltage source/picoammeters, in both inert and ambient atmospheric condition. CMS measurements are performed by a Vertex 80 v FTIR spectrometer in conjunction with a Hyperion 1000 confocal microscope from Bruker. Since FET device substrates are opaque to IR light, measurements are conducted in reflectance mode. CMS reflectance spectra are obtained in quasi-static mode as $-\Delta R/R = (R_{on} - R_{off})/R_{off}$ where R_{on} and R_{off} are reflectance spectra with gate bias V_{on} and V_{off}, respectively. Liquid nitrogen cooled, low noise MCT detector is used in the spectral range of 680 to 4000 cm^{-1} wavenumbers, with spectral resolution of 16 cm^{-1}. Averaging of 100 CMS spectra is used to increase signal to noise ratio. Phase resolution of 128 cm^{-1} is used during Fourier transformation. Spectra are acquired in ambient condition.

Computational method: The IR and Raman vibrational modes of extended π-conjugated polymer P3HT were studies by Density Functional Theory (DFT) calculations. All the calculations were carried out with Gaussian09 program using Becke three-parameter Lee-Yang-Parr hybrid functional (B3LYP) with 6–31 G(d) basis set. The geometry of neutral and charged molecules was fully optimized without symmetry constrains. The calculations were performed for finite length oligomers (10 repeat units) to mimic properties of the corresponding polymer.

1. Österbacka, R., An, C., Jiang, X. & Vardeny, Z. Two-dimensional electronic excitations in self-assembled conjugated polymer nanocrystals. *Science* **287**, 839–842 (2000).
2. Jiang, X. M. *et al.* Spectroscopic studies of photoexcitations in regioregular and regiorandom polythiophene films. *Adv. Funct. Mater.* **12**, 587–597 (2002).
3. Bakulin, A. A. *et al.* The role of driving energy and delocalized states for charge separation in organic semiconductors. *Science* **335**, 1340–1344 (2012).
4. Sirringhaus, H. *et al.* Two-dimensional charge transport in self-organized, high-mobility conjugated polymers. *Nature* **401**, 685–688 (1999).
5. Moses, D., Soci, C., Miranda, P. & Heeger, A. J. The role of electron photoemission in the photoconductivity of semiconducting polymers. *Chem. Phys. Lett.* **350**, 531–536 (2001).
6. Soci, C. *et al.* Photoconductivity of a low-bandgap conjugated polymer. *Adv. Funct. Mater.* **17**, 632–636 (2007).
7. Soci, C., Moses, D., Xu, Q.-H. & Heeger, A. J. Charge-carrier relaxation dynamics in highly ordered poly (p-phenylene vinylene): Effects of carrier bimolecular recombination and trapping. *Phys. Rev. B* **72**, 245204 (2005).
8. Brown, P. J., Sirringhaus, H., Harrison, M., Shkunov, M. & Friend, R. H. Optical spectroscopy of field-induced charge in self-organized high mobility poly(3-hexylthiophene). *Phys. Rev. B* **63**, 125204 (2001).
9. Zhao, N. *et al.* Polaron localization at interfaces in high-mobility microcrystalline conjugated polymers. *Adv. Mater.* **21**, 3759–3763 (2009).
10. Manaka, T., Kawashima, S. & Iwamoto, M. Evaluation of carrier density in organic field-effect transistor by charge modulated spectroscopy. *Jpn. J. Appl. Phys.* **50**, 04DK12 (2011).
11. Manaka, T., Kawashima, S. & Iwamoto, M. Charge modulated reflectance topography for probing in-plane carrier distribution in pentacene field-effect transistors. *Appl. Phys. Lett.* **97**, 113302–113303 (2010).
12. Itoh, E., Terashima, K., Nagai, H. & Miyairi, K. Evaluation of poly(3-hexylthiophene)/polymeric insulator interface by charge modulation spectroscopy technique. *Thin Solid Films* **518**, 810–813 (2009).
13. Bittle, E. G., Brill, J. W. & Anthony, J. E. Electro-optic measurement of carrier mobility in an organic thin-film transistor. *Appl. Phys. Lett.* **97**, 013302 (2010).
14. Khatib, O. *et al.* Infrared signatures of high carrier densities induced in semiconducting poly(3-hexylthiophene) by fluorinated organosilane molecules. *J. Appl. Phys.* **107**, 123702–123706 (2010).
15. Li, Z. Q. *et al.* Infrared imaging of the nanometer-thick accumulation layer in organic field-effect transistors. *Nano Lett.* **6**, 224–228 (2006).
16. Di Pietro, R., Fazzi, D., Kehoe, T. B. & Sirringhaus, H. Spectroscopic investigation of oxygen- and water-induced electron trapping and charge transport instabilities in n-type polymer semiconductors. *J. Am. Chem. Soc.* **134**, 14877–14889 (2012).
17. Xu, H. *et al.* Spectroscopic study of electron and hole polarons in a high-mobility donor–acceptor conjugated copolymer. *J. Phys. Chem. C* **117**, 6835–6841 (2013).
18. Chen, Z. *et al.* Origin of the different transport properties of electron and hole polarons in an ambipolar polyselenophene-based conjugated polymer. *Phys. Rev, B* **84**, 115211 (2011).
19. Caironi, M. *et al.* Very low degree of energetic disorder as the origin of high mobility in an n-channel polymer semiconductor. *Adv. Funct. Mater.* **21**, 3371–3381 (2011).
20. Sciascia, C. *et al.* Sub-micrometer charge modulation microscopy of a high mobility polymeric n-channel field-effect transistor. *Adv. Mater.* **23**, 5086–5090 (2011).
21. Meyertholen, A. D. *et al.* Concentration-dependent mobility in organic field-effect transistors probed by infrared spectromicroscopy of the charge density profile. *Appl. Phys. Lett.* **90**, 222108 (2007).
22. Ma, W., Yang, C., Gong, X., Lee, K. & Heeger, A. J. Thermally stable, efficient polymer solar cells with nanoscale control of the interpenetrating network morphology. *Adv Funct Mater* **15**, 1617–1622 (2005).
23. Sirringhaus, H., Tessler, N. & Friend, R. H. Integrated optoelectronic devices based on conjugated polymers. *Science* **280**, 1741–1744 (1998).
24. Sun, Y. M. *et al.* Polythiophene-based field-effect transistors with enhanced air stability. *Org. Electron.* **11**, 351–355 (2010).
25. Lin, S. W., Sun, Y. M. & Song, A. M. Enhanced stability of poly(3-hexylthiophene) transistors with optimally cured poly(methyl methacrylate) dielectric layers. *Synth. Met.* **160**, 2430–2434 (2010).
26. Brown, A. R., Jarrett, C. P., deLeeuw, D. M. & Matters, M. Field-effect transistors made from solution-processed organic semiconductors. *Synth. Met.* **88**, 37–55 (1997).
27. Horovitz, B. Infrared activity of peierls systems and application to polyacetylene. *Solid State Commun.* **41**, 729–734 (1982).
28. Osterbacka, R., Jiang, X. M., An, C. P., Horovitz, B. & Vardeny, Z. V. Photoinduced quantum interference antiresonances in pi-conjugated polymers. *Phys. Rev. Lett.* **88**, 226401 (2002).
29. Chabinyc, M. L., Street, R. A. & Northrup, J. E. Effects of molecular oxygen and ozone on polythiophene-based thin-film transistors. *Appl. Phys. Lett.* **90**, 123508 (2007).
30. Abdou, M. S. A., Orfino, F. P., Son, Y. & Holdcroft, S. Interaction of oxygen with conjugated polymers: Charge transfer complex formation with poly(3-alkylthiophenes). *J. Am. Chem. Soc.* **119**, 4518–4524 (1997).
31. Abdou, M. S. A., Orfino, F. P., Xie, Z. W., Deen, M. J. & Holdcroft, S. Reversible charge-transfer complexes between molecular-oxygen and poly(3-alkylthiophene)s. *Adv. Mater.* **6**, 838–841 (1994).
32. Hoshino, S. *et al.* Influence of moisture on device characteristics of polythiophene-based field-effect transistors. *J. Appl. Phys.* **95**, 5088–5093 (2004).
33. Socrates, G. Infrared and raman characteristic group frequencies: Tables and charts. (Wiley, Chichester, 2001).
34. Ostroverkhova, O. Handbook of organic materials for optical and optoelectronic devices: Properties and applications. (Woodhead Publishing Limited, Oxford, 2013).
35. Osterbacka, R., An, C. P., Jiang, X. M. & Vardeny, Z. V. Delocalized polarons in self-assembled poly(3-hexyl thiophene) nanocrystals. *Synth. Met.* **116**, 317–320 (2001).
36. Heeger, A. J., Sariciftci, N. S. & Namdas, E. B. *Semiconducting and metallic polymers.* (OUP, Oxford, 2010).
37. Bernier, P., Bidan, G. & Lefrant, S. *Advances in synthetic metals: Twenty years of progress in science and technology.* (Elsevier Science, Burlington, 1999).
38. Cho, S. *et al.* Thermal annealing-induced enhancement of the field-effect mobility of regioregular poly(3-hexylthiophene) films. *J. Appl. Phys.* **100**, 114503–114506 (2006).

Acknowledgments

Research was partially supported by the NTU NAP startup grant (No. M4080511) and by the Funding of Initiatives in Support of NTU 2015 (No. M58110092). We thank Dr. Heinrich Peter Diesinger for his help in setting up the CMS experiment and Dr. Behrad Gholipour for proof-reading the manuscript.

Author contributions

C.S. and M.C. generated the original idea; X.Y.C. and Z.W. built the experiment and collected data. J.Y. performed DFT calculations. X.Y.C. analysed the data. All the authors contributed to discussion of the results. The manuscript was written by X.Y.C., M.C. and C.S. C.S. supervised the work.

Additional information

Supplementary information accompanies this paper at http://www.nature.com/scientificreports

Competing financial interests: The authors declare no competing financial interests.

How to cite this article: Chin, X.Y., Yin, J., Wang, Z.L., Caironi, M. & Soci, C. Mapping polarons in polymer FETs by charge modulation microscopy in the mid-infrared. *Sci. Rep.* **4**, 3626; DOI:10.1038/srep03626 (2014).